JOURNAL OF MATERIALS SCIENCE 37 (2002) 2773–2780

The influence of laser annealing on the crystallization processes in amorphous Co-rich alloys

V. G. KRAVETS, X. PORTIER, A. K. PETFORD-LONG
Department of Materials, University of Oxford, Oxford OX1 3PH, UK
E-mail: vasyl_kravets@yahoo.com

Crystallization of Co-rich amorphous alloys via thermal and laser annealing has been studied using X-ray diffraction and high resolution electron microscopy techniques. It has been found that microstructural properties of the resulting alloys can differ significantly for the two thermal treatments depending on their Co content. $Co_{78}Fe_2Mn_2Si_9B_9$, $Co_{72}Fe_8B_{20}$ and $Co_{50}Fe_{28}Si_{10}B_{12}$ amorphous alloys have been studied and only $Co_{72}Fe_8B_{20}$ has shown very different crystallization processes after thermal and laser annealing. The results of comparative analysis of the influence of laser and thermal annealing on optical and structural properties of the samples are discussed.

1. Introduction

Amorphous ribbons of soft ferromagnetic alloys have attracted considerable attention over the past few years because of their unique physical properties and potential technological applications. For application of these materials a detailed knowledge of the crystallization and kinetic behavior is very important [1]. Annealing process of metallic ribbons at temperatures considerably below the crystallization temperature produces irreversible structural changes in the material, resulting in changes in many of the physical properties, some drastically and other only to a moderate degree [1, 2]. For example, Co-rich amorphous alloys have shown a five-fold increase in initial magnetic permeability and in the giant magnetoimpedance effect upon controlled thermal annealing at temperatures lower than the crystallization temperature [3, 4].

The crystallization processes in Co-rich amorphous ribbons under thermal annealing are well studied, but process occurring during laser annealing is still not fully understood. Laser annealing can play a major role in the formation of the nanocrystallites in Co-rich amorphous alloys and be essential in changing the physical properties of the ribbons. The main advantages of laser annealing are rapid change of the properties in air and easier operation compared to thermal annealing. Laser annealing allows the conditions of the incident energy (pulse power, pulse duration, wavelength) to be changed over a wide range, that makes possible the formation on nanocrystallites of various sizes and shapes.

In this paper we report a characterization of the crystallization processes in $Co_{78}Fe_2Mn_2Si_9B_9$, $Co_{72}Fe_8B_{20}$ and $Co_{50}Fe_{28}Si_{10}B_{12}$ amorphous alloys transformed using thermal and laser annealing. Based on the assumption that the effect of laser irradiation is to increase temperature locally and very rapidly, we have compared the laser irradiated spot with films which were instantaneously annealed. In this work we showed that laser annealing is a good alternative method to produce controlled crystallization of amorphous materials. Laser heating can create uniform crystallization at temperature which is much higher than that reached by other methods. We demonstrated that the obtained film contains very fine grains and also new compositions. In this connection it should be expected to obtain nanocrystalline ferromagnetic materials with improved soft magnetic properties in comparison to similar composition materials with crystalline or amorphous structure.

2. Sample preparation and experiment

Ribbon samples of amorphous alloys were prepared by the melt spinning method. The amorphous structure of the ribbons was checked by X-ray diffraction. The composition of the alloys investigated was determined by Auger electron spectroscopy (AES). The content of each element in the samples corresponds to their chemical formula with an accuracy of 0.5%. Auger electron spectra were obtained with the sample at normal incidence to the analyzer and employing a primary beam voltage of 3 kV and a modulation of 3 eV peak-to-peak. The as-grown samples showed a contamination of the surface by C and O. The spectra of the polished samples of these alloys showed Auger peaks which are characteristic for the metals (Co, Fe) plus Si and B. A residual C peak was observed in the spectrum of the polished samples of CoFeSiB alloys with a very low intensity. The quantification was performed by measuring the peak heights for the LMM transitions in Co, Fe and the KLL transitions in C and O within the 500–900 eV range, and for the LMM transitions in Si and B at 50–400 eV. After correction using literature values for the relative sensitivity factors, the surface stoechiometry was found to be consistent with the nominal bulk composition.

The samples were irradiated along its longitudinal axis at a programmable velocity in air by Nd-YAG laser at wavelength of 1064 nm. The spatial profile of the beam at the sample site was determined by maximal and minimal beam width as 1.5 and 1.0 mm respectively. The running velocity of the laser beam was fixed at 5 cm/s, so that any point along the sample was directly irradiated during 0.03 s. The fluences at the maximum of laser power distribution were within the range of 0–150 mW. The fluence was determined to within 5–8%.

The temperature rise at the irradiated site for a ribbon is given [5–7]:

$$T(r,z) = \left\{P_0 t_{\text{pul}} \exp\left(-(r/r_0)^2\right) \exp(-\alpha z)\right\} \Big/ \left\{\pi \rho c_{\text{v}} r_0^2 d\right\} \quad (1)$$

where P_0 is the laser power, t_{pul} is the pulse duration, c_{v} is the heat capacity of amorphous alloy, ρ is the mass density, α is the absorption coefficient of the material at the given laser wavelength, d is the film thickness and r_0 is the laser beam radius. The temperature rise falls exponentially as one moves along the film thickness away from its surface at $z = 0$. The values of α for all three samples were found from ellipsometrical measurements in the near IR region. We have calculated the temperature enhancement at the center of the laser-irradiated spot, using Equation 1. For a laser density energy of 50 mJ/cm^2 the temperature estimated is about of 350°C. The ribbons which have been thermally annealed at about of 350°C during 1 hour have been kept in vacuum of $(1–3) \times 10^{-5}$ Torr. The annealing temperature was always lower than the crystallization temperature.

The evolution of the reflectivity and the complex refractive index $n' = n - ik$ of the irradiated surface are measured at wavelength $\lambda = 632.8$ nm using ellipsometry [8, 9]. The reflection coefficient is proportional to the degree of the crystallization χ which may be expressed by ratio:

$$\chi = (R - R_{\text{A}})/(R_{\text{C}} - R_{\text{A}}) \quad (2)$$

where R_{A}, and R_{C} are reflectivities for amorphous and crystalline phases, respectively. R is the reflectivity of the nanocrystallite alloys, which was obtained after laser annealing. Accurate ellipsometry measurements were performed to determine the functions R_{A}, R and R_{C}.

The ribbon microstructure was investigated using X-ray diffraction and high resolution electron microscopy (HREM) with a JEOL 4000EX microscope (point-to-point resolution limit of 0.16 nm) operated at 400 kV. The ribbon was glued on a copper ring and then ion-beam milled to electron transparency. All the TEM images presented below are plan-view images.

3. Results and discussion

As an example, Fig. 1 shows the composition distribution of Co, Fe, Si and B in a $Co_{50}Fe_{28}Si_{10}B_{12}$ film, obtained using AES. It can be seen that from 20 nm below the surface, Co, Fe, Si and B are homogeneously distributed, and the amount of every element is consistent with the nominal bulk composition. The chemical composition for the three samples is essentially the same and remains so for varying film thicknesses. The sample surface is enriched by metalloid Si and B atoms. It can be seen that the Si(B) : Co, Si(B) : Fe ratio decrease with the film depth.

Fig. 2 shows the value χ as a function of the energy density of the incident laser pulse (curve 1—$Co_{78}Fe_2Mn_2Si_9B_9$; curve 2—$Co_{72}Fe_8B_{20}$ and curve 3—$Co_{50}Fe_{28}Si_{10}B_{12}$). At low laser energy density the reflectivity changes only slightly for $Co_{72}Fe_8B_{20}$ and $Co_{50}Fe_{28}Si_{10}B_{12}$ alloys. For sample of $Co_{78}Fe_2Mn_2Si_9B_9$ alloy the reflectivity seems to be

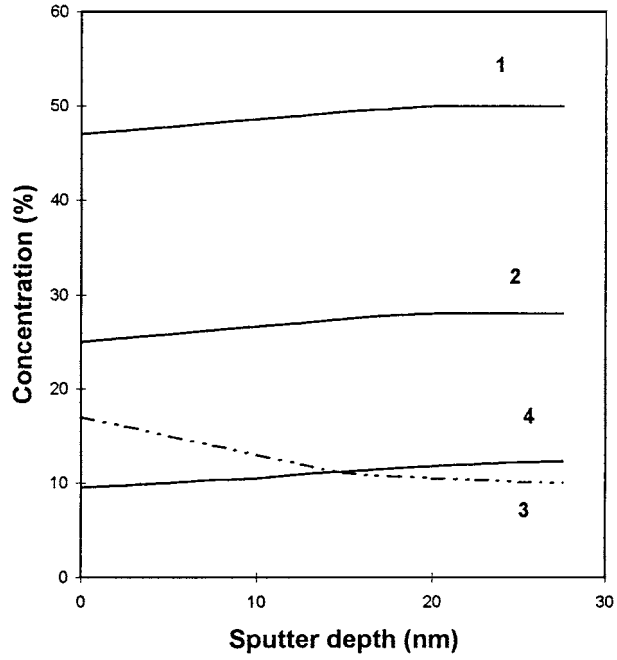

Figure 1 The composition distribution of Co (1), Fe (2), Si (3), and B (4) in a $Co_{50}Fe_{28}Si_{10}B_{12}$ film, obtained using AES.

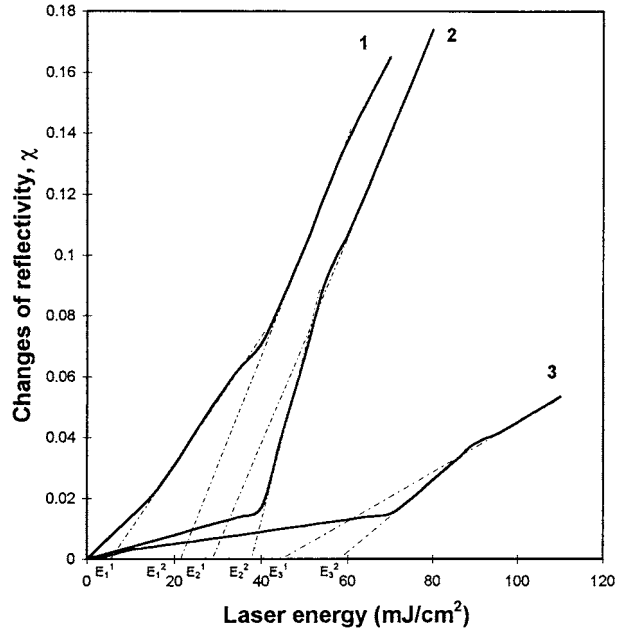

Figure 2 The degree of the crystallization χ as a function of the energy density of incident laser pulse (curve 1—$Co_{78}Fe_2Mn_2Si_9B_9$; curve 2—$Co_{72}Fe_8B_{20}$, curve 3—$Co_{50}Fe_{28}Si_{10}B_{12}$).

changed at all incident laser energy densities. By increasing the energy density of the laser pulse, a linear rise in the reflectivity signals and χ is observed. The reflectivity is rapidly changed whereas laser density energy is about of 37 mJ/cm^2 and 60 mJ/cm^2, for $Co_{72}Fe_8B_{20}$ and $Co_{50}Fe_{28}Si_{10}B_{12}$ alloys respectively. The function $\chi(J)$ consists of two different lines, which have distinct slopes for these alloys (Fig. 2). One may see that process of crystallization occurs in two stages. By extending these lines towards the abscissa axis, as shown in Fig. 2 by dashed lines, the intersection with the abscissa for each slope can be determined (labeled as E_i^j). We may assume that these energies correspond to the appropriate activation energy values for crystallization in each case. We can see that the process of crystallization occurs in two stages. The value of the activation energy for the crystallization process under laser irradiation in $Co_{50}Fe_{28}Si_{10}B_{12}$ alloy may be estimated as one from 2 to 3.5 eV. For $Co_{72}Fe_8B_{20}$ alloy this value is order of (2.6 ± 0.6) eV. The activation energies obtained in this manner for laser annealing process of Co-rich amorphous ribbons show a decrease of second crystallization step in comparison with $Co_{50}Fe_{28}Si_{10}B_{12}$ alloy. For the latter the highest value of the activation energy is observed that agrees with data in work [10]. A two-stage process of crystallization must be accompanied by the formation of α-(Co, Fe) phase, in a first step, and also by the formation of an eutectic intermetallic phase (Co, Fe)$_3$(Si, B) [10–12]. Depending on the chemical composition of these metallic glasses, a suitable sequence for the crystallization process was proposed and the activation energies of the first (3.5–5 eV) and second (2–3.5 eV) crystallization stages were also estimated.

Figs 3–5 show plan-view TEM and HREM images and selected area electron diffraction patterns for $Co_{50}Fe_{28}Si_{10}B_{12}$, $Co_{72}Fe_8B_{20}$ and $Co_{78}Fe_2Mn_2Si_9B_9$, respectively, after heat treatment at 350°C for 1 hour (Figs 3a, 4a, and 5a) and after laser annealing at 50 mJ/cm^2 that corresponds to about 350°C (Figs 3b, 4b and 5b). In a first approach, one can notice that for Co-rich alloys, laser annealing produces greater structural changes in comparison with thermal annealing especially for the $Co_{72}Fe_8B_{20}$ and $Co_{78}Fe_2Mn_2Si_9B_9$ alloys. TEM observations confirm the crystallization of small grains in these alloys. In Fig. 3 one can notice the very similiar configuration of the $Co_{50}Fe_{28}Si_{10}B_{12}$ ribbons after thermal (Fig. 3a) and laser (Fig. 3b) annealing. The films are polycrystalline with an average grain size of about 50 nm. For $Co_{72}Fe_8B_{20}$ ribbons, the two annealing processes lead to very different structural properties as shown in Fig. 4a (thermal annealing) where big grains (∼70 nm) are formed, whereas much smaller grains (∼20 nm) within much bigger grains (∼1 μm) have grown after laser annealing (Fig. 4b). Thermal annealing performed on the $Co_{78}Fe_2Mn_2Si_9B_9$ ribbons leads to a polycrystalline film with very small grains of a few nanometers (some are indicated by arrows in Fig. 5a) and laser annealing (Fig. 5b) gives rise to much larger grains (∼50 nm) embedded in an amorphous matrix according to the selected area diffraction pattern shown inset in Fig. 5b.

The intensity of the diffracted rings in the electron diffraction patterns in each case, allowed an identification of the present phases after laser and thermal annealing. The phases associated with the measured interplanar distances from HREM images (not shown) are presented in Tables I–III.

TABLE I Diffraction patterns of crystallized $Co_{50}Fe_{28}Si_{10}B_{12}$ ribbons

Thermal annealing 350°C			Laser annealing		
d_{obs} (nm)	(*hkl*)	Phase	d_{obs} (nm)	(*hkl*)	Phase
0.353	111	fcc Co	0.353	111	fcc Co
0.288	110	α-Fe	0.288	110	α-Fe
0.283	111	bcc α-Fe(CoSi)	0.283	111	bcc α-Fe(CoSi)
0.203	111	β-Co	0.203	111	β-Co
0.201	021	CoB	0.201	021	CoB
0.201	210	Co_3B	0.201	210	Co_3B
0.127	110	α-Co	0.127	110	α-Co

TABLE II Diffraction patterns of crystallized $Co_{72}Fe_8B_{20}$ ribbons

Thermal annealing 350°C			Laser annealing		
d_{obs} (nm)	(*hkl*)	Phase	d_{obs} (nm)	(*hkl*)	Phase
0.353	111	fcc Co	0.353	111	fcc Co
0.308	111	Co_3B	0.288	110	α-Fe
0.288	110	α-Fe	0.283	111	bcc α-Fe(CoSi)
0.258	200	Co_2B	0.258	200	Co_2B
0.252	$\{01\ \bar{1}0\}_{hcp}$	Co	0.245	021	Co_3B
0.245	021	Co_3B	0.240	200	Co_2B
0.240	200	Co_2B			
0.220	002	Co_2B	0.220	002	Co_2B
0.203	111	β-Co			

TABLE III Diffraction patterns of crystallized $Co_{78}Fe_2Mn_2Si_9B_9$ ribbons

Thermal annealing 350°C			Laser annealing		
d_{obs} (nm)	(*hkl*)	Phase	d_{obs} (nm)	(*hkl*)	Phase
0.353	111	fcc Co	0.353	111	fcc Co
0.288	110	α-Fe	0.288	110	α-Fe
			0.240	200	Co_2B $(CoFe)_2B$
0.203	111	β-Co	0.203	111	β-Co

The corresponding X-ray diffraction patterns are shown in Figs 6–8 (a—thermal, b—laser annealing). It is noteworthy that crystal growth is quite complex. The identification of the individual crystalline phases in hard because of the numerous lines in the X-ray diffraction spectra (see Figs 6–8). At first approximation it can be said that the crystalline phases are rather composed of α-Fe, α-Co, β-Co and various metal-metalloid phases. It may be seen that the X-ray diffraction patterns (Fig. 6a and b) and the TEM images (Figs 3a and b) obtained for thermal and laser annealed $Co_{50}Fe_{28}Si_{10}B_{12}$ alloys are very similar. This result confirms that the temperature reached upon laser annealing, which was estimated by Equation 1, was rather the same as for thermal annealing (350°C). The two major final products of the crystallization are α-Fe(Co, Si) and body-centered tetragonal $(CoFe)_2B$ phases (Figs 6–8), as usually found for CoFeSiB alloys [10–15]. For higher iron concentration (>8 at.%) the formation of α-Fe has been preceded the crystallization of Co-based phases. According to [14] the CoFeB alloys with more than

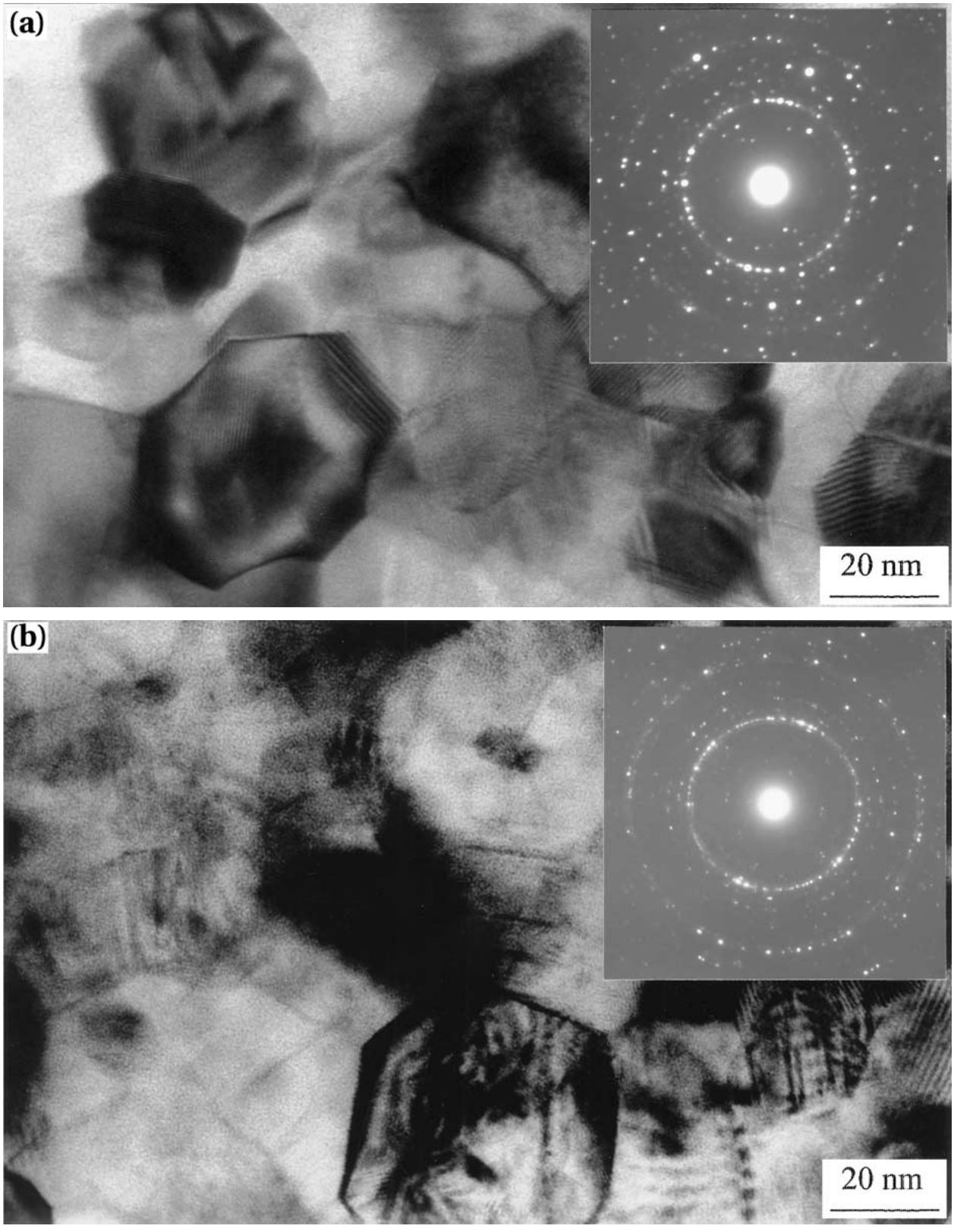

Figure 3 Plan-view HREM images and selected area electron diffraction patterns for $Co_{50}Fe_{28}Si_{10}B_{12}$ (a) after heat treatment at 350°C for 1 hour; (b) after laser annealing at 50 mJ/cm^2 that corresponds to about 350°C.

8 at.% of iron have been revealed the presence of α-Fe crystals with a distinctive shape (see Figs 6a and b) and then the formation of "eutectic" grains of β-Co + Co_3B. For the alloys containing the highest Co concentration (>60 at.%) the presence of the Co_2B phase was detected after crystallization of $Co_{72}Fe_8B_{20}$ and $Co_{78}Fe_2Mn_2Si_9B_9$ alloys. We may also see the presence of β-Co phase in these alloys, which had been previously revealed in [10–12], for low-iron CoFeBSi contained alloys. Transmission electron microscopy (TEM) and diffraction analyses have shown α-Co phase with a lattice parameter close to $a \sim 0.35$–0.36 nm.

For $Co_{78}Fe_2Mn_2Si_9B_9$ alloy (Fig. 8) one can see a broad peak for $2\theta = 46^\circ$ in both annealing processes. As it is known [10], thermal stability of amorphous alloy against crystallization monotonically decreases

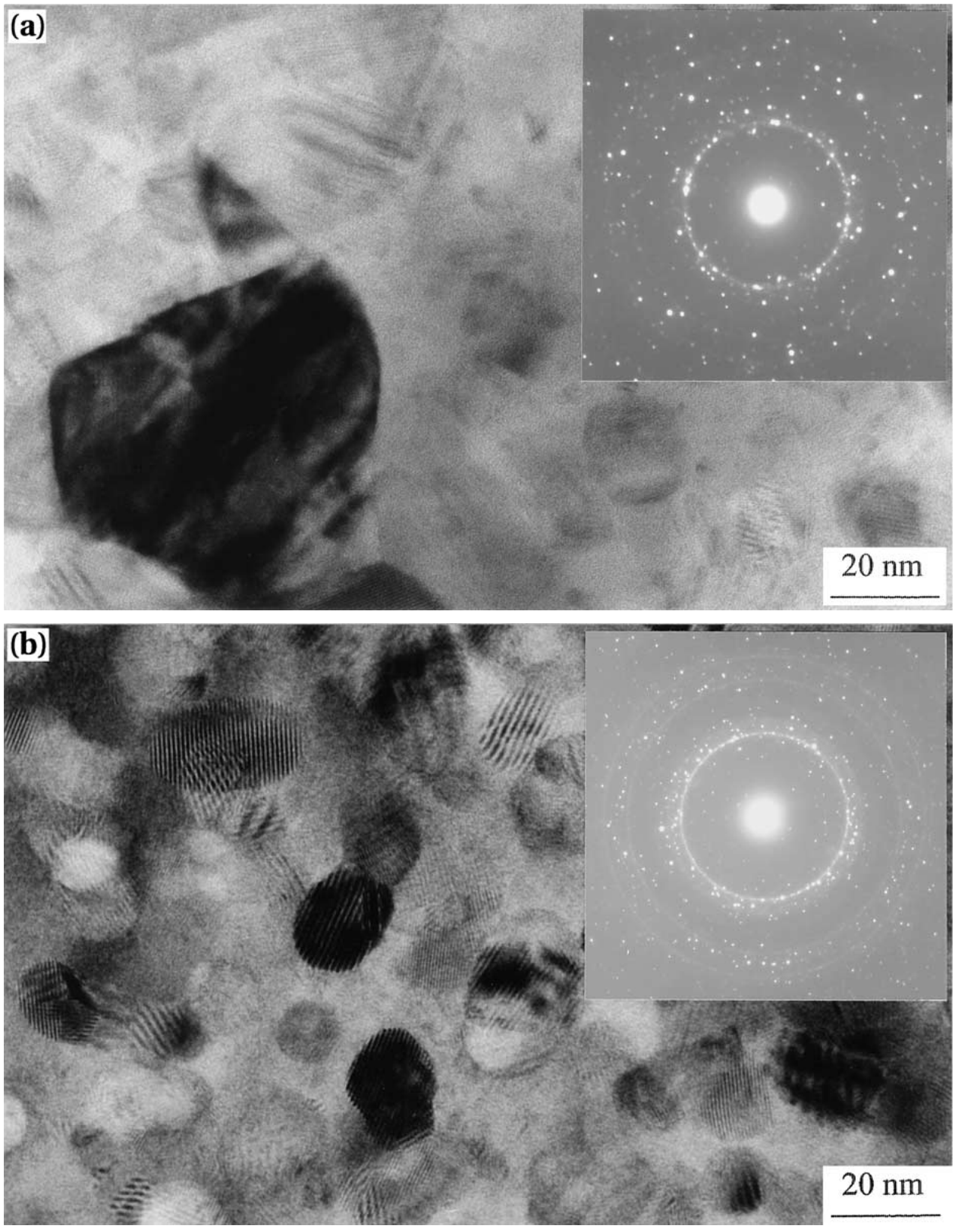

Figure 4 Plan-view HREM images and selected area electron diffraction patterns for $Co_{72}Fe_8B_{20}$ (a) after heat treatment at 350°C for 1 hour; (b) after laser annealing at 50 mJ/cm^2 that corresponds to about 350°C.

with the cobalt content in the material, as evidenced by the shift of the crystallization onset to lower temperature. However, the temperature of the crystallization increases essentially in CoFeBSi alloys doped by Mn, Ti and Cr. The samples partially crystallized show the presence of some crystalline phase lines identified as belonging to solid solution α-Fe, β-Co; $(CoFe)_2B$, and Co_2B [10–12]. These features are in good agreement with our result observed for the $Co_{78}Fe_2Mn_2Si_9B_9$ alloy where the crystallization process has not been fully completed. Nevertheless, it is worth noting that after laser annealing the $Co_{78}Fe_2Mn_2Si_9B_9$ ribbon is characterized by a greater degree of crystallization than after thermal annealing. We can see in Fig. 8b and in Table III, that the laser annealing process is accompanied by the formation of metal and metalloid phases.

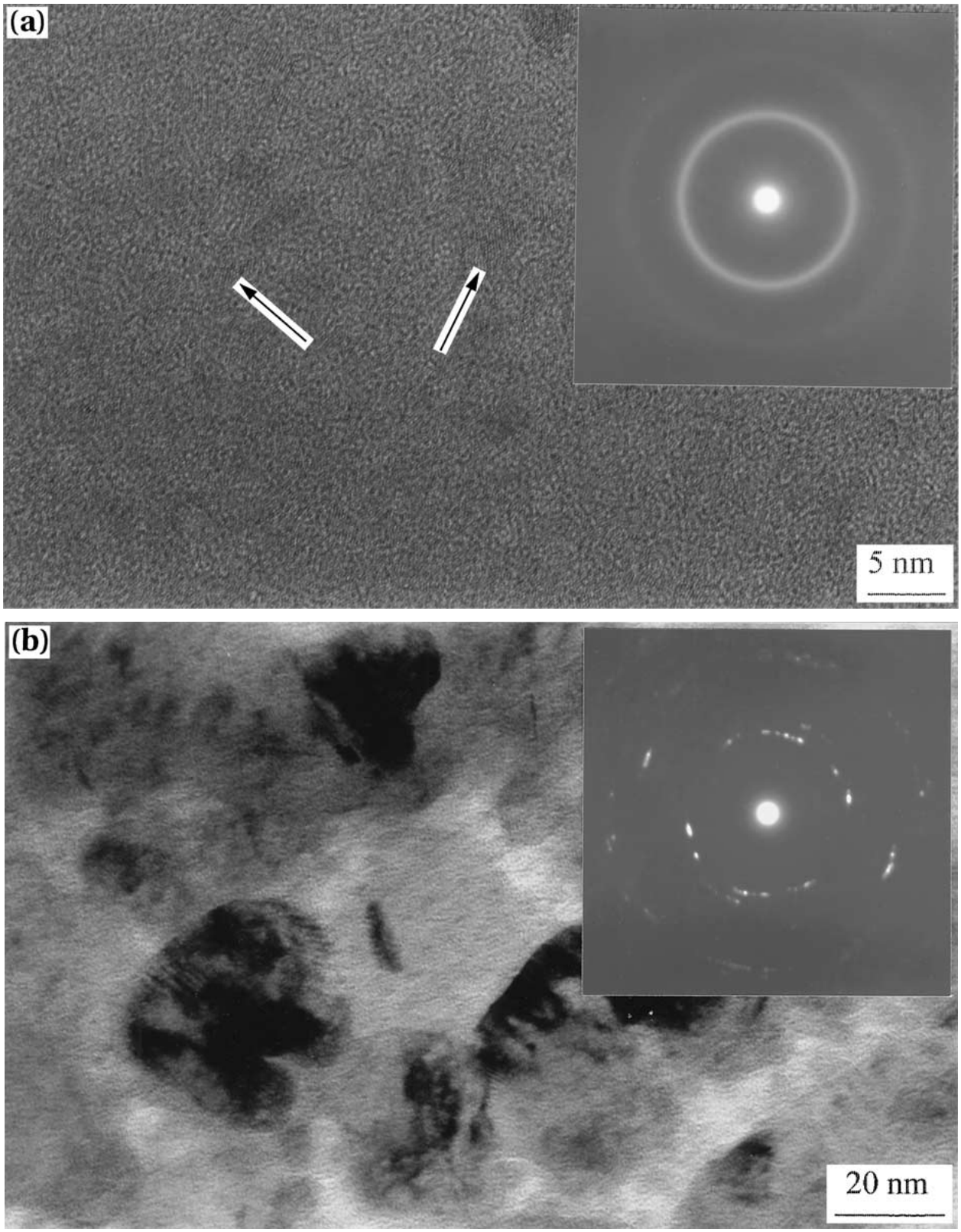

Figure 5 Plan-view HREM images and selected area electron diffraction patterns for $Co_{78}Fe_2Mn_2Si_9B_9$ (a) after heat treatment at 350°C for 1 hour; (b) after laser annealing at 50 mJ/cm^2 that corresponds to about 350°C.

We suggest that this is a result of the fact that during the process of laser annealing, the metal atoms absorb the most part of the energy that increases their mobility and diffusivity, and allows α-Fe, β-Co; $(CoFe)_2B$, and Co_2B phases to be produced. Metallic atoms in alloys can absorb more laser energy than metalloids atoms. For this reason the reflection coefficient changes to a greater degree for the $Co_{78}Fe_2Mn_2Si_9B_9$ alloy than for the $Co_{50}Fe_{28}Si_{10}B_{12}$, because the Co-rich amorphous alloys have a large absorption coefficient. We can see these changes by determining R as a function of laser energy (Fig. 2).

The structural properties of $Co_{72}Fe_8B_{20}$ alloy distinguish significantly after both thermal (Figs 4a and 7a) and laser (Figs 4b and 7b) annealing processes. After thermal annealing large uniform grains have grown

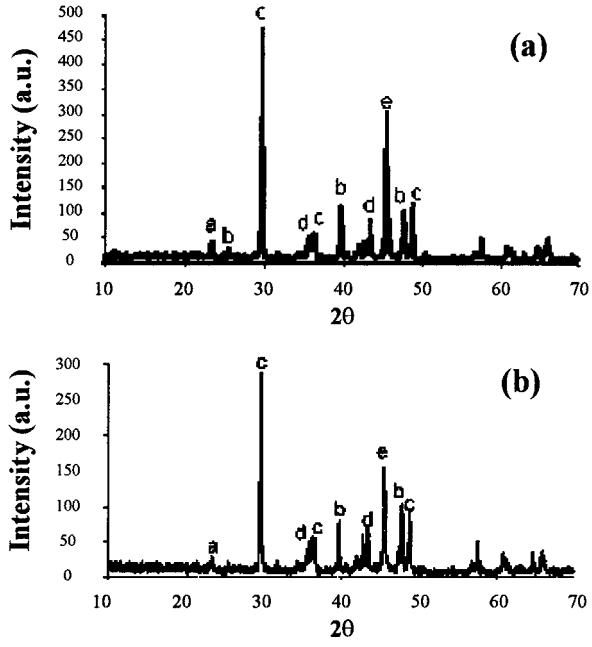

Figure 6 The intensity of X-ray diffraction pattern for $Co_{50}Fe_{28}Si_{10}B_{12}$ alloy after thermal (a) and laser (b) annealing: a-peak—α-Co; b-peak—β-Co; c-peak—α-Fe; d-peak—$(CoFe)_2B$; e-peak—Co_2B; f-peak—Co_3B.

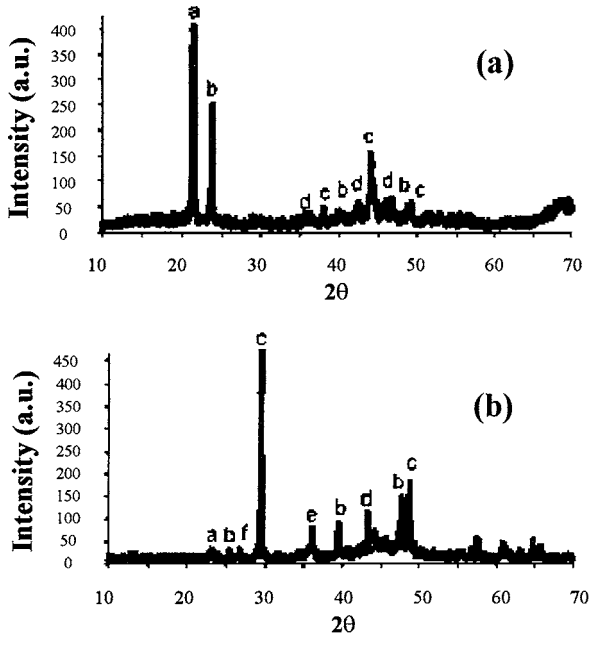

Figure 7 The intensity of X-ray diffraction pattern for $Co_{72}Fe_8B_{20}$ alloy after thermal (a) and laser (b) annealing: a-peak—α-Co; b-peak—β-Co; c-peak—α-Fe; d-peak—$(CoFe)_2B$; e-peak—Co_2B; f-peak—Co_3B.

(Fig. 4a) whose grain size is comparable to that of the grains formed after thermal or laser annealing for the $Co_{50}Fe_{28}Si_{10}B_{12}$ alloy (Fig. 3a and b). The formation of small grains within very big grains occurs only upon laser annealing process (Fig. 4b). These results show clearly the two steps crystallization process in these materials. As the Co content has increased, the activation energy has also increased and the thermal annealing procedure has not reached the two step crystallization process needed to obtain the full crystallization of the film. Laser annealing due to the rapid temperature change can produce uniform crystallization at a temperature which is much higher than that reached

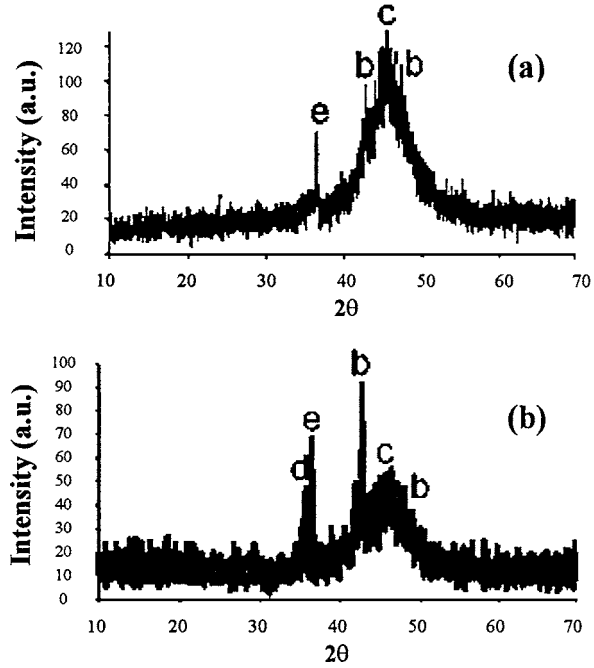

Figure 8 The intensity of X-ray diffraction pattern for $Co_{78}Fe_2Mn_2Si_9B_9$ alloy after thermal (a) and laser (b) annealing: a-peak—α-Co; b-peak—β-Co; c-peak—α-Fe; d-peak—$(CoFe)_2B$; e-peak—Co_2B; f-peak—Co_3B.

by other methods. Moreover, very fine grains and also new compositions appeared [16]. Our experimental results for $Co_{72}Fe_8B_{20}$ and $Co_{78}Fe_2Mn_2Si_9B_9$ confirm the formation of $(CoFe)_2B$ and α-Fe phases after laser annealing. The Co (Fe) atoms in laser annealing process can diffuse over long distances and therefore induce the growth of such phases as CoB, Co_2B, Co_3B and $(CoFe)_2B$ in $Co_{72}Fe_8B_{20}$ alloy. One may see from TEM measurements (Fig. 4b), that after laser annealing Co-rich alloys contain large grains with smaller precipitates. Our TEM and diffraction analyses have also shown the presence of the α-Co phase with a lattice parameter close to $a \sim 0.35$–0.36 nm in $Co_{72}Fe_8B_{20}$ alloy.

4. Conclusion

1. It was shown that the laser annealing causes changes of the optical and structural properties of Co-rich amorphous alloys in a greater degree than thermal annealing.

2. The processes of crystallization under laser irradiation for CoFeSiB amorphous alloys consist of two stages. For Co-rich amorphous alloys after laser annealing the value of the activation energy is found to be smaller than for the Fe-rich amorphous alloys.

3. The Co-rich ribbon films for both annealing treatments have been found to be not fully crystallized but a greater degree of crystallization has been noticed after laser annealing.

References

1. A. VAN DEN BEUKEL, in "Rapidly Solidified Materials," edited by P. W. Lee and S. Carbonera (ASM, New York, 1986) p. 193.
2. A. L. GREER, in "Rapidly Solidified Alloys: Processes Structure, Properties, Applications," edited by H. H. Liebermand (ASM, New York, 1993) p. 269.
3. P. QUAINTANA, E. AMANO, R. VALENZUELA and J. T. S. IRVINE, *J. Appl. Phys.* **75** (1994) 6940.

4. L. V. PANINA, K. MOHRI, K. BUSHIDA and M. NODA, *ibid*. **76** (1994) 6198.
5. J. SIEGEL, J. SOLIS, C. N. AFONSO and C. GARCIA, *ibid*. **80** (1996) 6677.
6. R. HUBER, M. KOCH and J. FELDMANN, *Appl. Phys. Lett*. **73** (1998) 2521.
7. P. ARUN, A. G. VEDESHWAR and N. C. MEHRA, *J. Phys. D: Appl. Phys*. **32** (1999) 183.
8. R. M. A. AZZAM and N. M. BASHARA, in "Ellipsometry and Polarized Light" (North-Holland, Amsterdam, 1977) p. 577.
9. W. A. MEGAHAN, Z. S. SHAN, A. M. MASSENGALE, T. E. TIWALD and J. A. WOOLLAM, *J. Vac. Sci. Technol.* A **7** (1989) 1271.
10. J. FILIPECKI, Z. MANDECKI, C. F. CONDE and A. CONDE, *J. Mater. Sci*. **33** (1998) 2171.
11. M. KOPCEWICZ, M. E. ZAYAT and U. GONSER, *J. Magn. Magn. Mater*. **72** (1988) 119.
12. G. A. STERGIOUDIS, J. YANKINTHOS, P. J. RENTZEPERIS, Z. BOJARSKI and T. J. PANEK, *J. Mater. Sci*. **27** (1992) 2468.
13. P. DUHAJ, P. SVEC, M. DURCEKOVA and G. VLASAK, *Mater. Sci. Eng*. **97** (1988) 337.
14. M. L. TRUDEAU, J.-Y. HUOT and R. SCHULZ, *J. Appl. Phys*. **67** (1990) 2333.
15. I. BETANCOURT, M. JIMENEZ, S. ABURTO, V. MARQUINA, R. GOMEZ *et al*., *J. Magn. Magn. Mater*. **140–144** (1995) 459.
16. L. LANOTTE and V. IANNOTTI, *J. Appl. Phys*. **78** (1995) 3531.

Received 20 April 2001
and accepted 25 February 2002